F29 Atomic Force Microscopy

Fortgeschrittenen Praktikum,

14.08.2025

Participants: **Jonathan Rodemers, Maria Susdorf**

Abstract

Atomic Force Microscopy (AFM) makes the observation of structures on a nano scale, too small to observe by optical means, possible. In this experiment, suboptimal P and I values (of the AMF feedback system) and their effects were observed and compared to optimal values (as seen in Fig. 3.2), which were then used for the rest of the experiment. The images of two calibration grids (seen in Fig. 3.4) were taken using the AFM to test its limitations. The step width, height and angle for each grid were determined (see Tab. 3.2).

After getting familiar with the setup, a CCD chip, the bright and dark sides of a nano lattice and various disc types (burned and pressed CDs, a DVD and a Blu-ray) were observed to determine their properties and explain the workings behind them. The storage capacities for the various disc types were estimated as well.

The results for the height and width of the pixels of the CCD chip can be found in section 3.3.1. Results for geometrical parameters for both sides of the nano lattice are listed in Tab. 3.3, while the results for the storage discs can be found in Tab. 3.4. All relevant parameters were able to be determined, matching literature values (in cases where there were any to be found). Unfortunately, some samples in this part appeared to have been mislabeled.

The formula derived for storage capacity estimates appeared to be inaccurate, the exact cause of which is not known given the resources provided by the lab course. However, the estimates were still close to the expected values. The storage capacity estimates can be found in Tab. 4.3.

Contents

1. Introduction

The following sections are largely based on the provided manual for this experiment. [1]

1.1 Observing Nano-Structures

Structures even tinier than the typical wavelength of visible light can't be observed through optical means. Instead, interaction between the sample and the microscope has to be recorded on an atomic scale. Microscopy based on this idea is called scanning probe microscopy (SPM), which was first developed in 1981 with the invention of scanning tunneling microscopy (STM) by Binnig and Rohrer. Only five years later, in 1986, Binnig, Quate and Gerber developed atomic force microscopy (AFM), also called scanning force microscopy (SFM).

STM works by measuring the tunneling current through a potential barrier. Provided this barrier is constant and of finite height, this tunneling current is proportional to e^{-d}, with d being the width of the potential barrier. The exponential relation means that even small changes in d can drastically alter the measured tunneling current, making this method extremely sensitive. Assuming a chemically homogeneous sample, the measured tunneling current can then directly be used to determine the sample's thickness. However, this only works for conducting samples.

Due to its mechanical nature, AFM can be used on conducting as well as non-conducting samples. Observing various samples using AFM will be the focus of this experiment.

1.2 Theoretical Principles behind AFM

Similarly to STM, AFM uses a very small tip that is brought up close to the sample. However, in contrast to STM, this tip is on a cantilever, which is deflected according to the forces that act on it. Those forces will be discussed later. The deflection of the cantilever can then be measured by an optical system, which then sends its signal to a feedback system that controls the position of the sample, keeping a controlled quantity constant (e.g. force, controller height, etc.) depending on the current operation mode. Modes will also be discussed in more detail later.

Using those principles, the AFM can scan the surface of a sample in a previously selected range, recording the changes needed to keep the controlled quantity constant at each point. Those changes are then used to build up a height - map picture.

1.2.1 Van der Waals interaction

One of the most important forces to consider here are the Van der Waals forces, since they are present in every operation mode. It is the primary force that attracts the tip to the surface, independent of what materials the tip or the sample are made of. This force is caused by fluctuations of electron density, which create temporary dipoles in the atoms making up the tip and the sample. Due to electrostatic influence, those dipoles again induce dipoles in the atoms nearby, which then attract each other. On an atomic scale, this attraction is described with the Lennard-Jones potential, which decreases with $\propto d^{-6}$ for short distances and even faster for larger distances, when retardation becomes relevant (i.e. the time used to travel the distance between the atoms being larger than the typical timescale of the fluctuations which caused the dipoles to occur).

In AFM, this potential can't be used as-is, since it only describes a single atom, not the tip or the sample, which are made up of significantly more atoms. For this reason, the Van der Waals potentials have to be integrated over all atoms which they are made of. To simplify this, different, simpler geometries are used for an approximation. The sphere over half-sphere model is the most common one, which approximates a spherical tip with radius R above an infinitely large surface. In this case, the potential can be written as

$$U = -\frac{HR}{6}\frac{1}{d} \tag{1.1}$$

Here, H is referring to the Hamaker constant, which depends on the material properties of the tip and the surface, and d is referring to the distance between the two. This equation is important because it shows that the force now decreases with d^{-1} instead of d^{-6}, as would be the case for single atoms. That means the Van der Waals interaction is significantly stronger over longer distances than in the case of the single atom.

This sphere-half sphere approximation is widely used in AFM theory, because it approximates the actual shape of the tip and the sample very well. With this potential, the microscope can achieve high resolution imaging, since even small changes in distance d lead to a measurable change in force. Still, compared to STM, the sensitivity is lower because the dependence on distance is much weaker than with tunnel current, which is proportional to e^{-d}. Nevertheless, Van der Waals forces and this approximation allow AFM to work in non-contact and tapping modes, which will be discussed later.

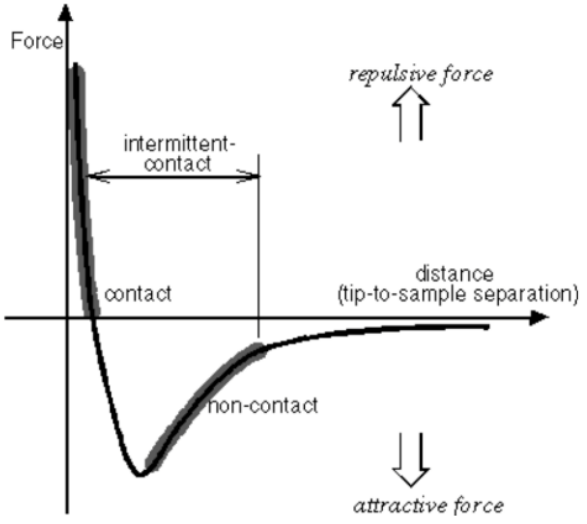

Figure 1.1: A typical force-distance curve with added classification of the AFM operation modes within the working regime of the Van der Waals potential. Source: FP script for F29 [1]

Shown above is the typical tipsample interaction force versus the distance d between them. For large d, very little force is present. Then, when the tip moves closer, the Van der Waals attraction becomes stronger and the interaction force becomes negative (attractive). At very small distances, Pauli repulsion starts to primarily affect the tip-sample interaction, with the force becoming infinitely repulsive as d approaches 0.

1.2.2 Attractive and repulsive Forces

The tip of the cantilever experiences different forces as it approaches the sample's surface. Some of these forces are attractive, while others are repulsive. What forces actually act on the tip strongly depends on the distance to the sample and on the AFM environment (e.g. air, vacuum, liquid, etc.).

The most universal force is the Van der Waals force, which is always attractive, as mentioned in the previous section.

In the right conditions, capillary forces can also play a large role. A small water droplet can form between the tip and the surface, which would pull them closer to each other. This force is also attractive and often stronger than the Van der Waals force if humidity is high.

Electrostatic forces can be both attractive or repulsive, depending on the charges of the tip and the sample. If they are charged differently, one being positive and the other negative, the force is attractive, if they are charged the same way, it is repulsive.

When the tip is very close to the surface, the chemical bonding forces become relevant. These are attractive because the atoms from the tip and the sample can form bonds with each other, fusing them together. This only happens at very short distances (i. e. on an atomic scale).

Finally, if the tip is too close to the surface, Pauli repulsion dominates. This force is caused by the exclusion principle of electrons, which do not allow their wave functions to overlap. It creates a very steep, repulsive force in the force-distance curve, which is undefined at $d = 0$.

The entire curve has a minimum, where attraction is strongest, and a steep rise where the repulsive forces dominate.

1.3 Operation Modes

Modes can be categorized as static or dynamic modes. In static modes, the tip stays in close contact with the sample's surface, while dynamic modes make the tip oscillate, be it in the non-contact range or touching the surface periodically.

Mode	**Function**	**Advantages**	**Disadvantages**
Static Modes (Contact Modes)	• tip always in close contact • repulsive force on tip • force of order 10^{-9} N	• very fast • high resolution of topography	• frictional forces can damage sample and/or tip
Dynamic Modes	• tip vibrates in and out of interaction range of Van der Waals potential • VdW interaction potential is superimposed • spring constant k modified by VdW contribution f ⇒ different resonance frequency	• steep resonance curves with springs with low damping ⇒ accuracy • preserves the materials used	• smaller deflections compared to contact modes ⇒ high accuracy needed • slower than static modes

Table 1.1: Comparison of static vs. dynamic modes.

Using those concepts, the following modes can be derived by keeping the controlled quantity, e. g. force or z-position, constant:

Mode	**Function**	**Advantages**	**Disadvantages**
Constant Height (static)	• sample set to constant height • deflection of cantilever detected by optical system	• fast, suited for flat samples	• really bad for non-flat samples • can be the most damaging mode
Constant Force (static)	• force is constant (deflection of cantilever doesn't change) • required controller changes recorded	• direct record of topology	• limited by response time of feedback circuit ⇒ slower
Non-Contact (dynamic)	• amplitude or resonance frequency held constant by moving sample up and down • controller changes are recorded • force of order 10^{-12}	• direct record of topology • doesn't damage sample and/or tip	• small forces, small deflections ⇒ high precision needed
Tapping (dynamic)	• like non-contact mode, but tip touches surface at the end of each oscillation cycle (intermittent contact)	• more sensitive than non-contact • no friction like in contact	• not many, method of choice in most experiments
Peak Force Tapping (dynamic)	• like tapping mode, but operates far below resonance frequency ⇒ $F(d)$-diagram at each pixel • peak force used as input for feedback system ⇒ directly controllable parameter	• $F(d)$-diagram can be used to determine other properties (e.g. adhesion)	• slower than tapping mode

Table 1.2: Comparison of different operation modes.

This experiment will be using tapping mode due to it having the advantages of being fairly accurate while not damaging the tip and sample.

1.4 Operation Principles

1.4.1 Optics

As shown in the previous section, all operation modes require measuring the cantilever's deflection in some way, be it for direct information of the sample's topology or to keep the cantilever at the same deflection (e.g. for constant force mode). To measure the deflection accurately, an optical system with lasers and a photosensitive detector is most commonly used.

The back of the cantilever is coated with reflective material (most commonly, gold or aluminum are used). The laser beam pointing at the back of the cantilever can then be reflected, with the direction of the reflected beam depending on the cantilever's horizontal and vertical deflection angles. The photosensitive detector can then measure the position of the reflected beam, making the computation of the deflection of the cantilever possible.

In this experiment, a four-quadrant photo diode will be used as the photosensitive detector. The four quadrants generate voltages proportional to the light shining on them. Using basic geometry and the law of reflection, the deflection can be obtained from this. The difference of voltage between upper and lower quadrants can be used to gain height information and the difference from the left and right ones to gain information about the twist of the cantilever. In modes where the cantilever oscillates, the system displays the RMS amplitude of the sinusoidal signal, which represents the average oscillation amplitude of the cantilever.

1.4.2 Feedback Control

Many operation modes need to adjust the z-position of the controller (i.e. its height) to keep a controlled quantity constant. For this, a feedback system is used, which has the measured deflection as an input and the adjustment of the z-position as an output.

This experiment uses a PID-feedback loop. The parameters P and I correspond to the proportional and integral components of the feedback controller that keeps force or amplitude constant during scanning. The term P determines how strongly the system reacts to the current error, i.e. the difference between the setpoint and the measured signal. The I term accounts for accumulated error over time, compensating for slow drifts or offsets.

2. Means of Measurement

2.0 Standard Procedure for Measurements

All data of this experiment was measured using a NanoWizard AFM [2]. This system consists of an optical microscope (for better vision of the general area to be scanned), an AFM and its provided software for taking measurements and looking through both microscopes.

The optical microscope was used to set up each sample for scanning. First, the tip had to be located to be visible on the connected camera feed. Then, the sample was focused on to look for a relatively clean scannable area. Once such an area has been found, the tip was brought into focus again. De-focusing again so that the plane focused on would be slightly closer to the sample, one can now bring up the sample until it comes into focus. Repeating this very carefully allows the tip to approach the sample's surface faster than if to only engage the tip using the provided software.

All images were taken with a 512×512 px resolution and a scanning frequency of 1 Hz.

2.1 P and I values

To get familiar with the experiment's setup, the "TGZ02" sample was observed first using a slightly used tip. The system auto-tuned the drive amplitude and frequency to match the cantilevers resonance peak. The resonance curve of the tip was recorded. Initially, this resonance curve was not sharp enough, threatening to make the results obtained with it unusable. However, this changed after scanning the sample once or twice, after which the resonance curve became sharper.

Suitable P and I values were found through trial and error. The suitability was determined through optimizing both traced and retraced curve overlap and the amount of noise. To directly compare them to unsuitable values, traced and retraced curves of optimal, too low and too high values were recorded. An image of the sample while the values were being changed was also taken.

2.2 Tip Characterization and Limitations of the AFM

Since the orientation of the steps of "TGZ02" was already known from images recorded in the previous part, it was known that they were satisfyingly perpendicular to the scanning direction. A full scan of the sample on a 10 ţm ×10 ţm area in this orientation was completed. Then, the scanning angle was changed by 90 degrees using the AFM software. A 10 ţm ×10 ţm scan of "TGZ02", roughly parallel to its steps, was completed as well.

During the change to the sample "TGZ01", the tip was broken accidentally and was replaced by a new one. A new calibration was completed and the corresponding resonance curve has been recorded.

Approximating the scanning direction so that the steps of "TGZ01" would be satisfyingly perpendicular to the scanning direction, an area of 10 ţm ×10 ţm was scanned and recorded.

Gwyddion, a free program used for SFM data visualization and analysis, was used to flatten the data, remove noise and place cursors on the height profile manually to measure the features of the sample (see [3]). All their uncertainties were determined by the standard deviation of measurements of different steps and the tolerable range for every single measurement's cursor placement.

In this case, step height, step width and step angle were measured using the software.

2.3 Samples

All samples were observed using the standard procedure (as mentioned in section 2.0) and evaluated with Gwyddion. Relevant differences are mentioned below. The AFM pictures of all samples can be found in the results.

2.3.1 CCD Chip

As has been done for the calibration grids, the "CCD" sample was scanned on a 10 ţm ×10 ţm area. The lattice constant of the pixel grid and the pixel height were measured.

2.3.2 Nano Lattice

Because the structures on a nano lattice are much smaller compared to the previous structure, a smaller scan area (1.5 ţm ×1.5 ţm) was chosen to achieve a higher resolution. The depth of holes in the lattice, their diameter and the distance between two holes were measured, both for the bright and the dark side.

2.3.3 Pressed CD, DVD and Blu-ray

To be able to compare and understand different disk storage mediums, pictures of a ”pressed CD”, a ”DVD” and a ”Blu-ray” sample were recorded on a 8.2 ţm ×8.2 ţm area. Because the first Blu-ray sample produced very unusual results, another Blu-ray sample has been recorded as well. The height, length and width of visible features of each sample were measured. Distance between tracks and track height (if present) were measured as well.

2.3.4 Burned CD

Finally, to compare a pressed CD to a burned CD on a nano scale, the ”burned CD” sample was scanned on a 5 ţm ×5 ţm area. Since the AFM image was very similar to the second ”Blu-ray” sample, but was of much worse quality, only feature height, track height and the distance between tracks were taken for this sample. Feature width and length were omitted since their uncertainties were too large and the measurements themselves wouldn't provide relevant additional info. This decision will be elaborated upon.

3. Results

3.1 P and I values

The resonance curves of the old tip (which was broken accidentally) and the new tip were exported and are displayed below.

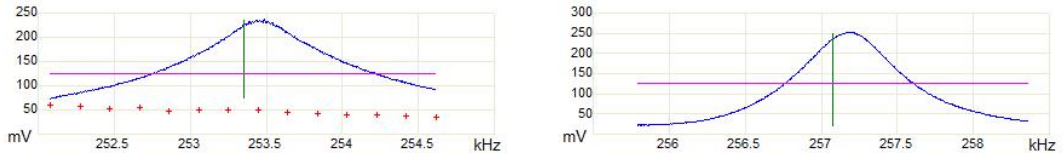

(a) old tip **(b)** new tip

Figure 3.1: Resonance curves using old tip (left) and brand new tip (right).

A sharper curve implies lower damping and cleaner oscillation of the cantilever. This means that newer cantilevers, which should have less damping because they aren't damaged by usage yet, should produce sharper curves. This coincides with differences seen between the older tip (Fig. 3.1a) and the newer one (Fig. 3.1b).

Tracing and retracing the curves with different P and I values, the following graphs were exported from the provided AFM software.

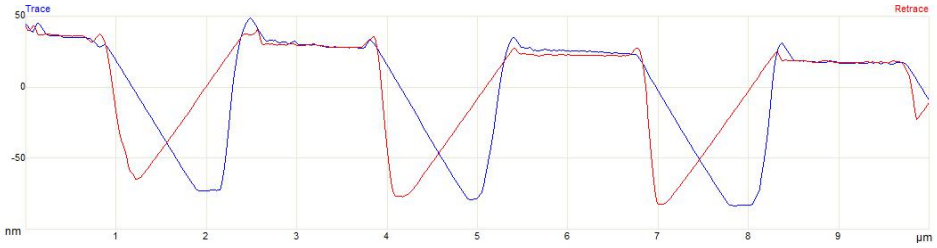

(a) $P = 3$, $I = 1$ (too low, as seen by the lack of overlap between steps)

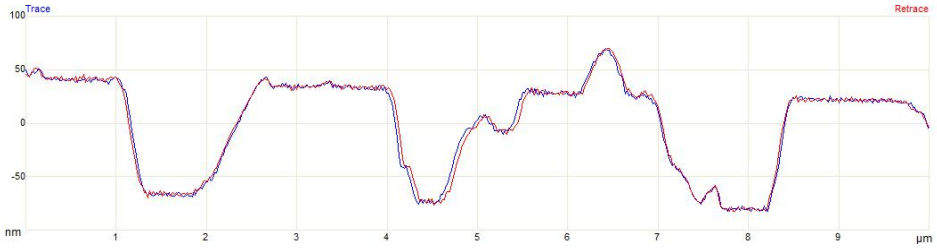

(b) $P = 15$, $I = 35$ (too high, as seen by the additional noise)

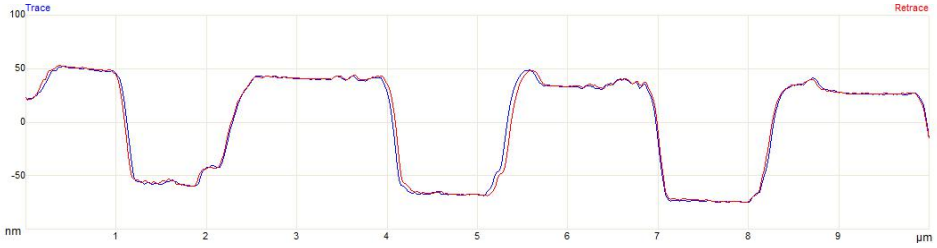

(c) $P = 12$, $I = 9$ (optimal)

Figure 3.2: Comparison of traced and retraced curves for different P and I values (from top to bottom): low values, high values, optimal values.

Values which were too high made the equipment create a noticeable noise, similar to a high pitched chip-tune note. Since P and I values amplify the system response, resonances in the controller can lead to noise, both visually in the AFM image and acoustically.

While the P and I values were being changed, an image of the "TGZ02" sample using those values was recorded, allowing a comparison of their effects within the same image. Higher values made the image sharper, but also caused more artifacts to appear, while low values smudged the image in the scanning direction.

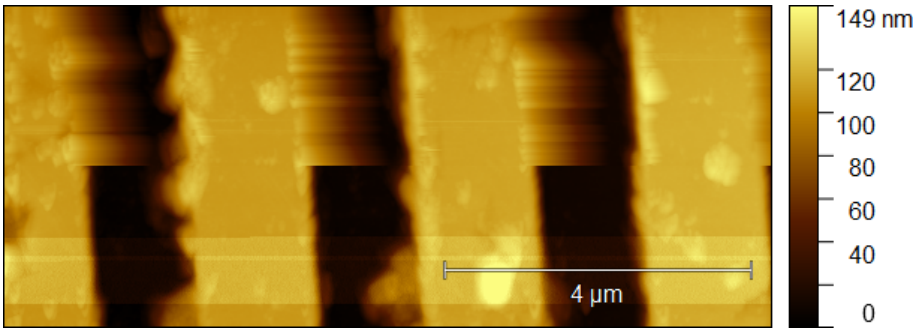

Figure 3.3: Values were changed while scanning was in progress. From top to bottom, the following four strips are visible: low values, optimal values, high values, optimal values.

3.2 Tip Characterization and Limitations of the AFM

To determine the grating characteristics of the provided calibration samples, "Gwyddion" was used as described in section 2.0.

The sample "TGZ01" showed significant differences between the step angles depending on which direction the angle was measured from (i. e. in positive or negative x-direction).

Sample	**Angle Left φ_l**	**Angle Right φ_r**
TGZ01 (perpendicular)	(24.78 ± 1.11) ř	(14.34 ± 0.46) ř

Table 3.1: Step angle data as measured for TGZ01, both from the left and the right side of each step.

The angle measured from the left, φ_l, was chosen to represent the measured step angle of "TGZ01" for reasons elaborated on in the discussion.

Different scanning directions and calibration grids produced the results below.

Sample	**Step Width w**	**Step Height h**	**Angle φ**
TGZ01 (perpendicular)	(2.87 ± 0.08) ţm	(20.4 ± 0.8) nm	(24.78 ± 1.11) ř
TGZ02 (perpendicular)	(2.98 ± 0.08) ţm	(106.2 ± 2.6) nm	(34.01 ± 2.19) ř
TGZ02 (parallel)	(3.04 ± 0.05) ţm	(103.2 ± 0.9) nm	(31.37 ± 1.92) ř

Table 3.2: All measurements taken relating to calibration grids.

A visual comparison of the samples can be found below. The structures are clearly identifiable. Some dirt appears to be on all of the samples, which is to be expected, since on this scale, even the tiniest impurity will still have a noticeable impact on the height profile.

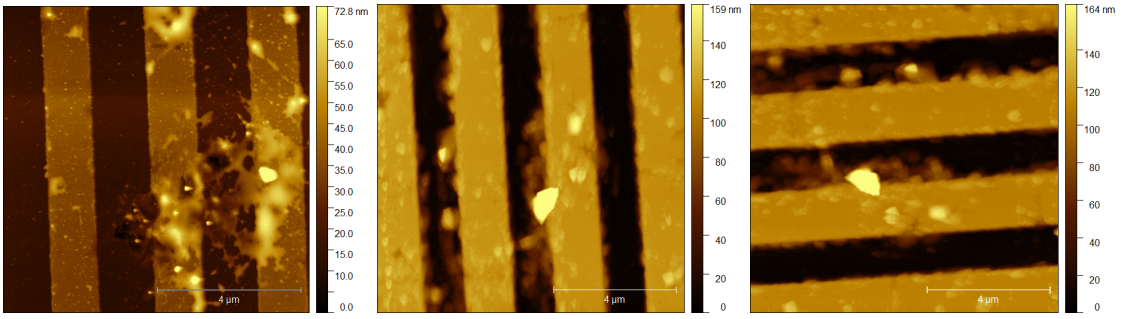

(a) TGZ01, perpendicular **(b)** TGZ02, perpendicular **(c)** TGZ02, parallel

Figure 3.4: Comparison of calibration grids under AFM with different scanning directions.

3.3 Samples

3.3.1 CCD Chip

The height h_{CCD} and the width w_{CCD} of each pixel were determined to be:

$$h_{\text{CCD}} = (546.9 \pm 6.2) \text{ nm} \qquad w_{\text{CCD}} = (2.294 \pm 0.086) \text{ ţm}$$

Together, red, green and blue (RGB) light can be combined to produce any visible color. However, each pixel on a CCD sensor is typically sensitive to only one of these wavelengths, meaning that a single pixel cannot record the full RGB color information. To work around this issue, CCD chips place pixels with different colors next to each other. Since the pixels lie so close together, the human eye can't tell individual pixels apart (i. e. "mixes" them), resulting in an image that appears to contain all wavelengths, not only RGB. The human eye functions similarly using cone cells.

Therefore, images in color require 3× more pixels than a black and white image, where only brightness is detected.

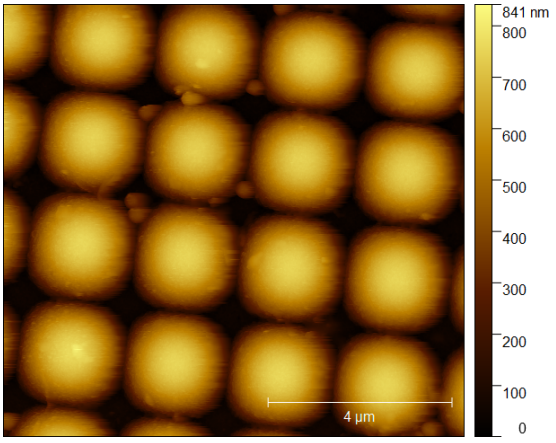

Figure 3.5: Individual pixels of a CCD chip under AFM.

Although the pixels are rounded instead of perfectly square, which differs from the idealized shape, this deviation doesn't make a difference on a macroscopic scale.

3.3.2 Nano Lattice

The bright and dark sides of the nano lattice shared the same pattern of evenly spaced holes on a lattice of equilateral triangles. The dark side's pattern was visibly larger, essentially being a "scaled-up" version of the bright side's pattern. This resulted in similar values for hole depth, but visibly different ones for hole diameter and distance between features (measured from the end of one hole to the start of the next).

Lattice side	Depth	Diameter	Distance between features
bright	(195.1 ± 3.0) nm	(170 ± 7) nm	(153 ± 4) nm
dark	(172.3 ± 1.3) nm	$(336 \pm 11$ nm	(269 ± 9) nm

Table 3.3: Feature sizes for nano lattice sample, both sides.

Also, as seen in the picture of the bright side of the nano lattice, one of its holes appears to be plugged. This has a negligible optical effect, but is worth mentioning as an example of a surface defect.

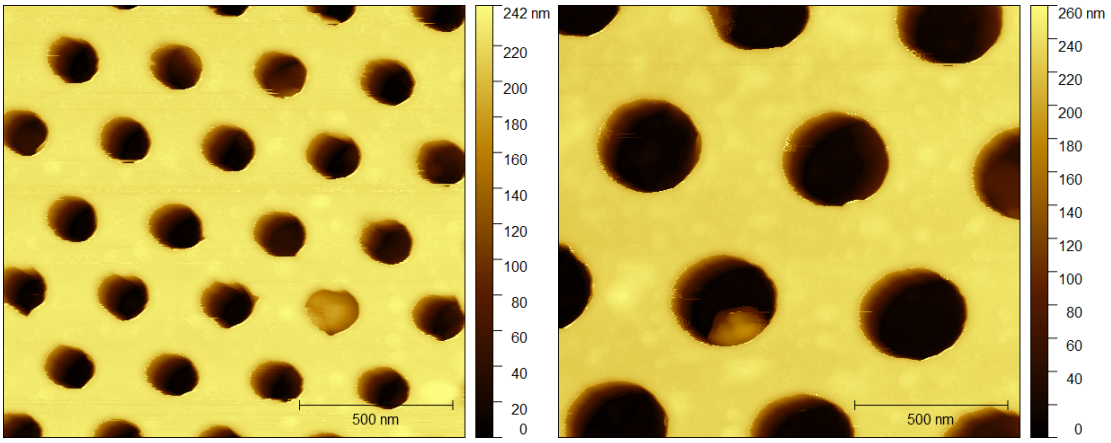

(a) bright side **(b)** dark side

Figure 3.6: Nano-lattice under AFM, bright side (left) and dark side (right).

If the lattice constant were to be reduced to only a few Ångstroms and the holes were occupied by atoms of the same species, the pattern of the lattice would suggest the surface of the fcc(111) face of an fcc crystal.

3.3.3 Pressed CD, DVD and Blu-ray

Every sample had features that presented as rounded shapes, which were either protruding or indented depending on disc type. Features appeared to lie on evenly spaced radial lines, which will be referred to as ”tracks” from now on. The features appeared to have the length of roughly a multiple of a base length. The same holds for the length of sections of the track without features.

For the pressed CD, the DVD and both Blu-ray samples, the measured feature characteristics are listed in the table below.

Sample	**CD (pressed)**	**DVD**	**Blu-ray #1**	**Blu-ray #2**
Feature height [nm]	179.80 ± 0.08	100.5 ± 6.3	105.1 ± 2.7	-56.54 ± 0.51
Feature width [nm]	363 ± 31	224 ± 18	223 ± 16	132 ± 12
Min. feature length [nm]	788.9 ± 82.8	394.6 ± 15.4	395.5 ± 16.0	145.4 ± 7.4
Track height [nm]	128.42 ± 0.08	-	-	-
Track distance [ţm]	1.448 ± 0.014	0.737 ± 0.010	0.719 ± 0.035	0.324 ± 0.011

Table 3.4: Comparison of ”pressed CD”, ”DVD” and ”Blu-ray” samples.

The larger relative errors for feature width and length is due to the blurriness of feature edges, which did not pose a problem for track distance or height measurements (i. e. measurements tangential to the plane).

The second Blu-ray sample is used in the following visual comparison of the different disk types.

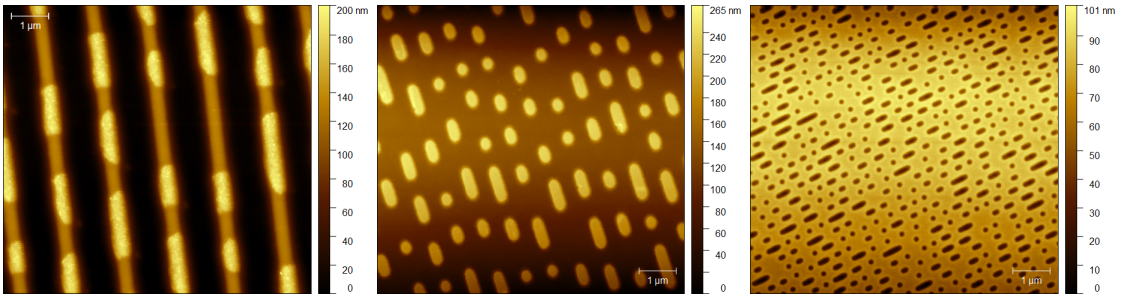

(a) "CD (pressed)" **(b)** "DVD" **(c)** "Blu-ray" (second sample)

Figure 3.7: Comparison of different disk types, from left to right: CD (pressed), DVD, Blu-ray.

Only the ”pressed CD” sample appeared to have elevated tracks. The features get smaller with increasing storage capacity. The second Blu-ray sample appears to be the only one to have an ”inverted” profile, in this case meaning that the features are deeper than the rest of the sample instead of the other way around.

Unlike the second Blu-ray sample, the first Blu-ray sample appeared to have striking similarities to the DVD sample, as shown below.

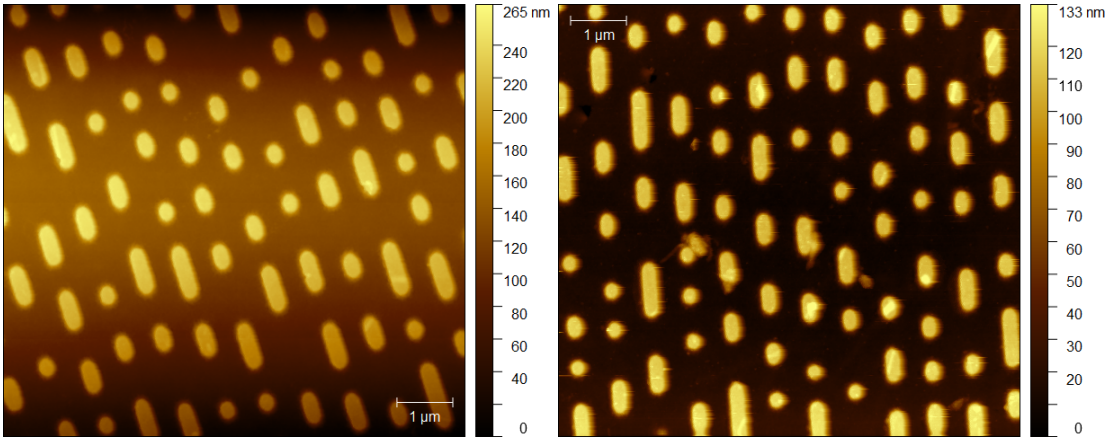

(a) "DVD" **(b)** "Blu-ray" (first sample)

Figure 3.8: Comparison of "DVD" sample and first "Blu-ray" sample.

The discrete lengths of features may lead to the conclusion that one feature could be interpreted as one bit, which would be read as either ”0” or ”1”, depending on whether a feature is present or not. This, however, is not how storage discs work.

Instead, when a laser reflects off a disc rotating at a constant speed, a jump from feature to non-feature (pits and lands) creates a phase shift, which is registered by a photo detector and interpreted as a ”1” channel bit. A section for which there are no changes is interpreted as ”0” channel bits, the number of which depends on the length of the section. The formats require that every ”1” has to be followed by a ”0”, which means the minimum feature length should be double the base length to avoid a jump following right after a jump.

The surface used by two channel bits A_{c-bit} can be computed using the area spanned by the minimal feature length (which is twice the channel bit length, as mentioned before!) and the distance between tracks.

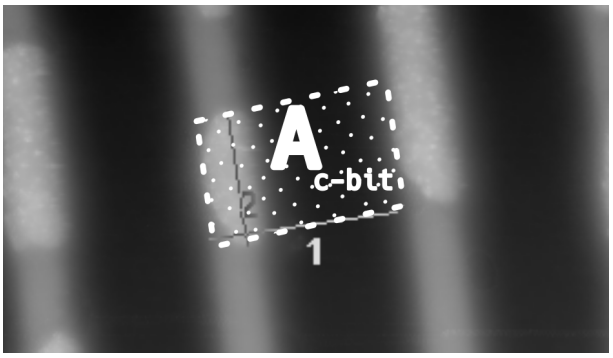

Figure 3.9: Visualization of the area of two channel bits, A_{c-bit}.

The number of channel bits on a disc can be approximated by dividing the total usable disc area (with inner radius r_{in} and outer radius r_{out}) by the calculated channel bit area $A_{c-bit}/2$.

$$N_{c-bits} \approx \frac{\text{disc area}}{\text{channelbit area}} = \frac{4\pi(r_{out}^2 - r_{in}^2)}{A_{c-bit}/2}$$

All disks appear to have the same radii, with:

$$r_{in} = (22.0 \pm 0.5)\text{mm} \qquad r_{out} = (58.0 \pm 0.5)\text{mm}$$

To estimate the usable storage capacity of a disc, the additional channel bits used for error correction have to be factored in. This is represented by the storage efficiency factor η, which represents the percentage of usable channel bits.

$$\eta_{\text{CD}} = 66\ \% \qquad \eta_{\text{DVD}} = 87\ \% \qquad \eta_{\text{Blu-ray}} = 81.7\ \%$$

The η values were calculated by subtracting the error overhead percentages from 1 (see [4], [5]).
Lastly, channel bits have to be converted to bits. For example, CDs use 8-14 modulation (EFM) with 3 additional security channel bits, which means that 14+3 channel bits are used to represent 8 data bits. DVD uses 16 to represent 8, Blu-ray 3 to represent 2 (see [4], [5]).
The final formula is comprised of all of those terms:

$$\text{Storage} = \eta \cdot \frac{\text{data bits}}{\text{channel bits}} \cdot \frac{4\pi(r_{out}^2 - r_{in}^2)}{A_{c-bit}/2}$$

This yielded the following results:

Sample	CD (pressed)	DVD	First Blu-ray	Second Blu-ray
Storage capacity [GB]	0.62 ± 0.07	3.38 ± 0.16	3.46 ± 0.23	26.15 ± 1.70

Table 3.5: Estimated storage capacities of observed disc samples.

3.3.4 Burned CD

A "burned CD" sample was scanned and recorded to determine the differences between a burned and a pressed CD. The latter sample was scanned in the previous section.

Sample	Feature height	Track height	Distance between repetitions
CD (burned)	(-52.4 ± 6.6) nm	no track	(0.336 ± 0.017) ţm
CD (pressed)	(179.80 ± 0.08) nm	(128.42 ± 0.08) nm	(1.448 ± 0.014) ţm
Second Blu-ray	(-56.54 ± 0.51) nm	no track	(0.324 ± 0.011) ţm

Table 3.6: Comparison of burned CD, pressed CD and second Blu-ray sample.

Due to striking similarities, the second "Blu-ray" sample has also been included in this table for comparison purposes. A visual comparison of the ”burned CD” and the ”Blu-ray” sample can be found below.

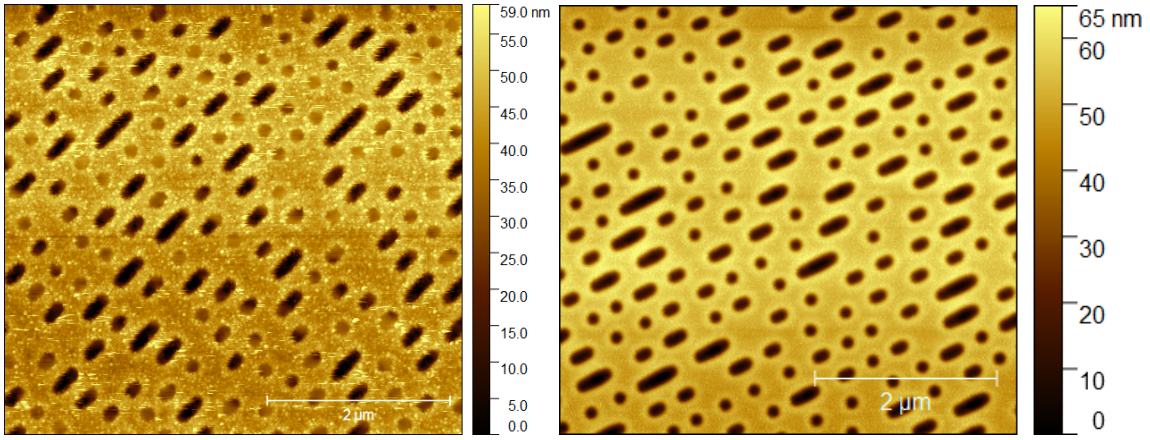

(a) "burned CD" **(b)** "Blu-ray" (second sample, cropped)

Figure 3.10: Comparison of "burned CD" sample and second "Blu-ray" sample, same scale.

4. Discussion

4.1 P and I values

Picking good P and I values by hand has the possibility of not picking the most ideal ones. For the accuracy of the experiment, however, the values chosen were good enough, producing relatively clean images.

Instabilities inside the AFM system as well as different outside parameters (e. g. different surface properties) could have the possibility of changing the optimal P and I values during the experiment. To solve this issue, automatic tuning functions can be employed. But again, given the accuracy of the experiment, this was not necessary.

4.2 Tip Characterization and Limitations of the AFM

During the change of the sample from ”TGZ02” to ”TGZ01”, the tip was broken and replaced by a new one with a much better resonance curve. Since a new AFM image for the ”TGZ02” sample has not been recorded, the importance of the sharpness of the curve can be seen when comparing the sharpness of the ”TGZ02” images to any other AFM image in this report.

As mentioned in the results for this part of the experiment, the step angles of the ”TGZ01” sample were different from each other depending on which direction they were measured from.

This may be due to topological defects of the tip, which can include the tip not being perfectly orthogonal to the surface. From one side, the tip would have no problem reaching nooks, while it would be blocked by the tilted rest of the tip from the other side. This explains why the angles stay the same for the traced and retraced curves, which would not be the case if the tip just wasn't lowered fast enough, as seen in the case of low P and I values where the curves don't overlap (see Fig. 3.2a).

The measured values agreed with the values provided in the manual:

Sample	**Step Width** w	**Step Height** h
TGZ01 (theoretical)	3.0 ţm	(18.0 ± 1.0) nm
TGZ01 (perpendicular)	(2.87 ± 0.08) ţm	(20.4 ± 0.8) nm
TGZ02 (theoretical)	3.0 ţm	(102.0 ± 1.5) nm
TGZ02 (perpendicular)	(2.98 ± 0.08) ţm	(106.2 ± 2.6) nm
TGZ02 (parallel)	(3.04 ± 0.05) ţm	(103.2 ± 0.9) nm

Table 4.1: Comparison of calibration grid parameters provided by the manual for this lab course (see [1]) vs. experimental values.

The possible tilt of the tip could also explain why the parallel scan produces a more accurate result for the step height, since a tilt in the scanning direction would affect measurements perpendicular to the steps more than a parallel ones.

4.3 Samples

4.3.1 CCD Chip

Since an AFM doesn't rely on optical means to observe samples, it can't display color either. This doesn't allow for the observation of the different pixel colors, which should be present since the chip belonged to a camera with the ability to take pictures in color.

Pictures of CCD sensors under an optical microscope visualize the different colors (RGB) and how they can be arranged.

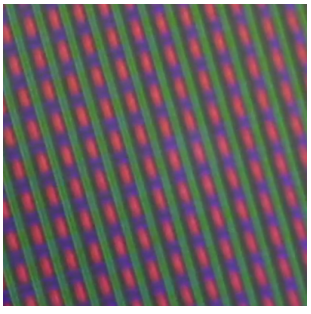

Figure 4.1: x80 microscope view of an RGGB Bayer filter on a 240 line Sony CCD PAL Camcorder CCD sensor (cropped, caption and image taken from Wikimedia Commons [6])

4.3.2 Nano Lattice

Smaller holes of a nano lattice mean that less light is "trapped " inside it, making it appear brighter than a nano lattice with larger holes. One of the holes of the bright side of the nano

lattice appeared to be plugged (see Fig. 3.6a), which has a negligible impact on the lattice's macroscopic appearance. However, it is a great example of a surface defect and highlights the importance of keeping AFM samples as clean as possible, since this hole is unlikely to be unplugged ever again.

4.3.3 Pressed CD, DVD and Blu-ray

The measured parameters were very close to the industry standard requirements. Only the track distance of the pressed CD deviated from its literature value more strongly than 1σ. A likely possible cause of this is unknown. A comparison of the experimental and theoretical values is displayed in Tab. 4.2.

The "DVD" matched the literature values, which highly suggests that this sample was an actual DVD. Unfortunately, the same could not be said about the first "Blu-ray" sample. Given the visual comparison of the "DVD" sample and the first "Blu-ray" sample (Fig. 3.8), in addition to their incredibly similar measured parameter values, the first "Blu-ray" sample is very likely to be a mislabeled DVD. This is supported by the second "Blu-ray" sample looking very different and having much smaller measured parameters which actually meet the industry standards for this disc type.

Sample	**Min. pit length [nm]**		**Track distance [ţm]**	
	experimental	theoretical	experimental	theoretical
CD (pressed)	788.9 ± 82.8	800	1.448 ± 0.014	1.6
DVD #1	394.6 ± 15.4	400	0.737 ± 0.010	0.74
DVD #2 ("Blu-ray")	395.5 ± 16.0	400	0.719 ± 0.035	0.74
Blu-ray	145.4 ± 7.4	150	0.324 ± 0.011	0.32

Table 4.2: Comparison of measured disc parameters with industrial standard (see [4]).

The formula for storage capacity produced results comparable to literature values, but given that the measured disc parameters were incredibly close to the industrial standard, one would have expected a more accurate result. The theoretical storage capacity using the formula was also computed, but produced different results than the actual theoretical storage capacities.

Sample	CD (pressed)	DVD #1	DVD #2 ("Blu-ray")	Blu-ray
Computed storage capacity [GB]	0.62 ± 0.07	3.38 ± 0.16	3.46 ± 0.23	26.15 ± 1.70
Computed storage capacity, theoretical parameters [GB]	0.55	3.32	3.32	25.67
Theoretical storage capacity [GB]	0.7	4.7	4.7	25

Table 4.3: Estimated storage capacities of observed disc samples.

This implies there were errors in the η-values of the disc types and/or errors inside the derived formula itself. Errors of the modulation factors or other parameters could also be possible, but considering that the η-values were incredibly hard to find, and even then not clearly identifiable to be correct, the problem is more likely to be caused by the latter (assuming the formula itself to be correct). In the future, it would be really helpful if the manual provided sources for those values to confirm whether the problem lies within the parameters or the formula itself.

4.3.4 Burned CD

Similarly to the first Blu-ray sample in the previous section, there were very strong and unusual similarities between samples of supposedly different data types. As visible in Fig. 3.10, the structures in the "Burned CD" sample and the second "Blu-ray" sample appear to be the same. Since the latter has been confirmed to be from an actual Blu-ray disk by the attending lab tutor, this strongly suggests that the "Burned CD" sample was also labeled incorrectly could actually be another Blu-ray sample instead.

Unfortunately, since no other burned CD samples were available, another attempt at scanning a confirmed burned CD was not possible.

Online research would suggest that that a burned CD would not appear to have physical pits and lands. Data on burned CDs is stored in dye or phase-change material instead, which changes its optical properties when heated by a laser. A differently refracted laser beam can reproduce the phase shift caused by pits and lands in the case of pressed CDs. In the case of rewritable CDs, this data can even be wiped and written again by reheating the entire disc (unlike pressed CDs, where one can only wipe the data by pressing the entire disc), which makes it more flexible in its usage, but also reduces its lifespan.

5. Summary

The resonance curves of an old and a new tip were recorded and confirmed that newer tips should show sharper resonance peaks. Low, high and optimal P and I values of the feedback system were found. The trace and retrace curves using those values were compared in Fig. 3.2. To obtain an accurate image and avoid damage to the AFM system, the optimal values found in this part were used for the rest of the experiment.

Pictures of the "TGZ01" and the "TGZ02" calibration grid were taken to determine the step width w, step height h and the step angle φ of both. Two pictures were taken of "TGZ02", with the steps perpendicular and parallel to the scanning direction, while only one was taken of "TGZ01", perpendicular to the scanning direction (for pictures, see Fig. 3.4). The measured parameters for the "TGZ01" sample were determined to be $h_1 = (20.4 \pm 0.8)$ nm, $w_1 = (2.87 \pm 0.08)$ µm and $\varphi_1 = (24.78 \pm 1.11)$ ř. For the "TGZ02" sample, the parameters for scans perpendicular and parallel to the steps were determined to be $h_\perp = (106.2 \pm 2.6)$ nm, $w_\perp = (2.98 \pm 0.08)$ µm, $\varphi_\perp = (34.01 \pm 2.19)$ ř and $h_\perp = (103.2 \pm 0.9)$ nm, $w_\perp = (3.04 \pm 0.05)$ µm, $\varphi_\parallel = (31.37 \pm 1.92)$ ř, respectively (see Tab. 3.2). All of those values agreed with the given parameters in the manual for this lab course [1].

Evaluating the AFM picture of the CCD chip sample, pixel height and width were determined to be $h_{\mathrm{CCD}} = (546.9 \pm 6.2)$ nm and $w_{\mathrm{CCD}} = (2.294 \pm 0.086)$ µm (as seen in section 3.3.1). Because

no info on the size of the chip itself was given, estimating the megapixels the camera (the chip originally belonged to) had was not possible.

The bright and dark side of a nano lattice were scanned. Both sides appeared to have holes on an equilateral triangular pattern, but on different scales (for pictures, see Fig. 3.6). Hole depth h, hole diameter d and the distance between holes x were measured and determined to be $h_{\text{bright}} = (195.1 \pm 3.0)$ nm, $d_{\text{bright}} = (170 \pm 7)$ nm, $x_{\text{bright}} = (153 \pm 4)$ nm for the bright side and $h_{\text{dark}} = (172.3 \pm 1.3)$ nm, $d_{\text{dark}} = (336 \pm 11)$ nm, $x_{\text{dark}} = (269 \pm 9)$ nm for the dark side (see Tab. 3.3).

The minimum pit length l and distance between tracks d for the pressed CD, DVD and Blu-ray samples were determined to be $l_{\text{CD}} = (788.9 \pm 82.8)$ nm, $l_{\text{DVD}} = (394.6 \pm 15.4)$ nm, $l_{\text{Blu-ray}} = (145.4 \pm 7.4)$ nm and $d_{\text{CD}} = (1.448 \pm 0.014)$ µm, $d_{\text{DVD}} = (0.737 \pm 0.010)$ µm, $d_{\text{Blu-ray}} = (0.324 \pm 0.011)$ µm. One sample labeled "Blu-ray" was highly likely to have been a DVD sample instead, with its parameters being $l_{\text{Blu-DVD}} = (395.5 \pm 16.0)$ nm and $d_{\text{Blu-DVD}} = (0.719 \pm 0.035)$ µm (for all values, see Tab. 3.4).

The storage capacities of the disc samples were estimated to be (0.62 ± 0.07) GB for a CD, (3.38 ± 0.16) GB for a DVD and (26.15 ± 1.70) GB for a Blu-ray (see Tab. 4.3). Since even the theoretical minimum pit lengths and track separation produced close, but inaccurate results, the derived formula for the estimate appeared to be inaccurate. A possible cause of this could be the lack of information about the storage efficiencies of different disc types available during the lab course.

Due to the "burned CD" sample having been a mislabeled Blu-ray sample and no actual burned CD samples were available, a comparison of burned vs. pressed CDs was not possible. A visual comparison between the "burned CD" and the confirmed Blu-ray can be found in Fig. 3.10.

Bibliography

[1] Universität Heidelberg. *F29: Atomic Force Microscopy*. 2015. URL https://www.physi.uni-heidelberg.de/Einrichtungen/FP/anleitungen/F29.pdf. [Last access: 15.08.2025].

[2] JPK Instruments. *NanoWizard AFM Handbook*. 2012. URL https://www.manualslib.com/manual/812468/Jpk-Instruments-Nanowizard.html. Version 2.2a, May 2012. [Last access: 15.10.2025].

[3] Gwyddion. *Gwyddion - Free SPM (AFM, SNOM/NSOM, STM, MFM, ...) data analysis software*. URL http://gwyddion.net/. [Last access: 20.08.2025].

[4] Ken C. Pohlmann. *Principles of Digital Audio, 6th Edition*. McGraw-Hill/Tab Electronics, 2010. ISBN 978-0-07-166346-5.

[5] Blu-ray Disc Association. *Physical Format Specifications for BD-RE, 5th Edition*. 2018.

[6] Dave L. Jones. Wikimedia Commons, 2012. URL https://commons.wikimedia.org/wiki/File:An_RGGB_Bayer_Colour_Filter_on_a_1980%27s_vintage_Sony_PAL_Camcorder_CCD.png. [Last access: 23.10.2025].